Journal of Alloys and Compounds 509 (2011) 8153–8157

Contents lists available at ScienceDirect

Journal of Alloys and Compounds

journal homepage: www.elsevier.com/locate/jallcom

Magnetic properties of a new iron lead vanadate $Pb_2FeV_3O_{11}$

N. Guskos [a,b], J. Typek [b,*], G. Zolnierkiewicz [b], R. Szymczak [c], P. Berczynski [b], K. Wardal [b], A. Blonska-Tabero [d]

[a] Solid State Physics, Department of Physics, University of Athens, Panepistimiopolis, 15 784 Zografos, Athens, Greece
[b] Institute of Physics, West Pomeranian University of Technology, Al. Piastow 48, 70-311 Szczecin, Poland
[c] Institute of Physics, Polish Academy of Sciences, Al. Lotnikow 36/42, Warszawa, Poland
[d] Department of Inorganic and Analytical Chemistry, West Pomeranian University of Technology, Al. Piastow 42, 70-065 Szczecin, Poland

ARTICLE INFO

Article history:
Received 6 April 2011
Received in revised form 26 May 2011
Accepted 30 May 2011
Available online 6 June 2011

Keywords:
EPR
Vanadates
Magnetic susceptibility

ABSTRACT

Temperature dependence of dc/ac magnetization and electron paramagnetic resonance (EPR) spectra of $Pb_2FeV_3O_{11}$ iron lead vanadate has been investigated. The dc magnetic measurements have shown the presence of antiferromagnetic interactions with Curie–Weiss temperature, $T_{CW} = -15.2$ K, in the high temperatures range while the field cooled (FC) magnetization revealed a maximum at $T_N = 2.5$ K which coincides with a long range magnetic ordering. Temperature dependence of χ' has shown a maximum at the same temperature. EPR spectrum of $Pb_2FeV_3O_{11}$ at room temperature is dominated by nearly symmetrical, very intense and broad resonance line centered at $g_{eff} \sim 2.0$ that could be attributed to the correlated system of iron ions. The temperature dependence of magnetic resonance parameters (amplitude, *g*-factor, linewidth, integrated intensity) has been determined in the 4–300 K range and it suggests the existence of short range correlated spin system up to high temperatures. The temperature dependence of the amplitude of the resonance line has shown a pronounced maximum at 12.5 K that indicates on the existence of two subsystems of weakly and strongly coupled iron pairs. Comparison of dc magnetic susceptibility and EPR integrated intensity points to the presence of correlated spin agglomerates that play an important role in determination of the magnetic response of $Pb_2FeV_3O_{11}$.

1. Introduction

Multicomponent vanadates M–Fe–V–O (M(II) = Mg, Zn, Mn, Cu, Ni and Co) exhibit very interesting physical (structural, magnetic and transport) and catalytic properties [1–14]. They belong to a group of useful catalysts used for the reaction of partial oxidation of organic compounds. Structural disorder, introduced by replacement of some magnetic ions in the sublattice of M(II) cations could results in an intense magnetic competition and frustration phenomena [9,10,15,16]. The above systems have displayed a very strong antiferromagnetic (AFM) interaction with very high values of the Curie–Weiss temperature, especially in compounds with Co(II) and Mn(II) magnetic ions.

Magnetic resonance measurements have shown that the above systems are approaching the phase with a long range magnetic order at high temperatures but dc magnetic susceptibility study has not shown the existence of such state even down to 3 K. The crystal structure of the system with Ni(II) magnetic ion at the cation position is not known and in this compound very complicated magnetic multiphase aggregate states are observed [17,18]. The temperature and frequency dependence of high frequency electron paramagnetic resonance (HF-EPR) spectra have shown that in $Mn_3Fe_4V_6O_{24}$ compound there is the coexistence of AFM with ferromagnetic (FM) interactions [10]. Recently, a new $Pb_2FeV_3O_{11}$ multicomponent vanadate was synthesized which crystallizes in higher crystallographic symmetry (monoclinic) than previously investigated $M_2FeV_3O_{11}$ (M(II) = Co, Mg and Zn) compounds (triclinic) [19].

The aim of this work is to study magnetic properties of a new $Pb_2FeV_3O_{11}$ lead vanadate in which the Pb^{2+} ion have a much greater radius than cations in other M(II) = Co, Mg, Ni, Zn vanadates. Dc/ac magnetic susceptibility and EPR methods will be employed. The obtained results will be compared with similar studies made on other $M_2FeV_3O_{11}$ vanadates.

2. Experimental

$Pb_2FeV_3O_{11}$ multicomponent vanadate was synthesized from an equimolar mixture of iron(III) orthovanadate(V) and lead(II) pyrovanadate(V): $FeVO_4 + Pb_2V_2O_7 = Pb_2FeV_3O_{11}$. Iron(III) orthovanadate(V) was obtained as a result of heating of equimolar mixture of Fe_2O_3 and V_2O_5 in three stages: 560 °C (20 h) + 590 °C (20 h × 2). Synthesis of lead(II) pyrovanadate(V) was performed during heating the stoichiometric mixture of $Pb(NO_3)_2$ and V_2O_5 in the following stages: 430 °C (20 h × 2) + 600 °C (20 h). The reactions were carried out by the conventional

* Corresponding author.
E-mail address: typjan@zut.edu.pl (J. Typek).

0925-8388/$ – see front matter © 2011 Elsevier B.V. All rights reserved.
doi:10.1016/j.jallcom.2011.05.114

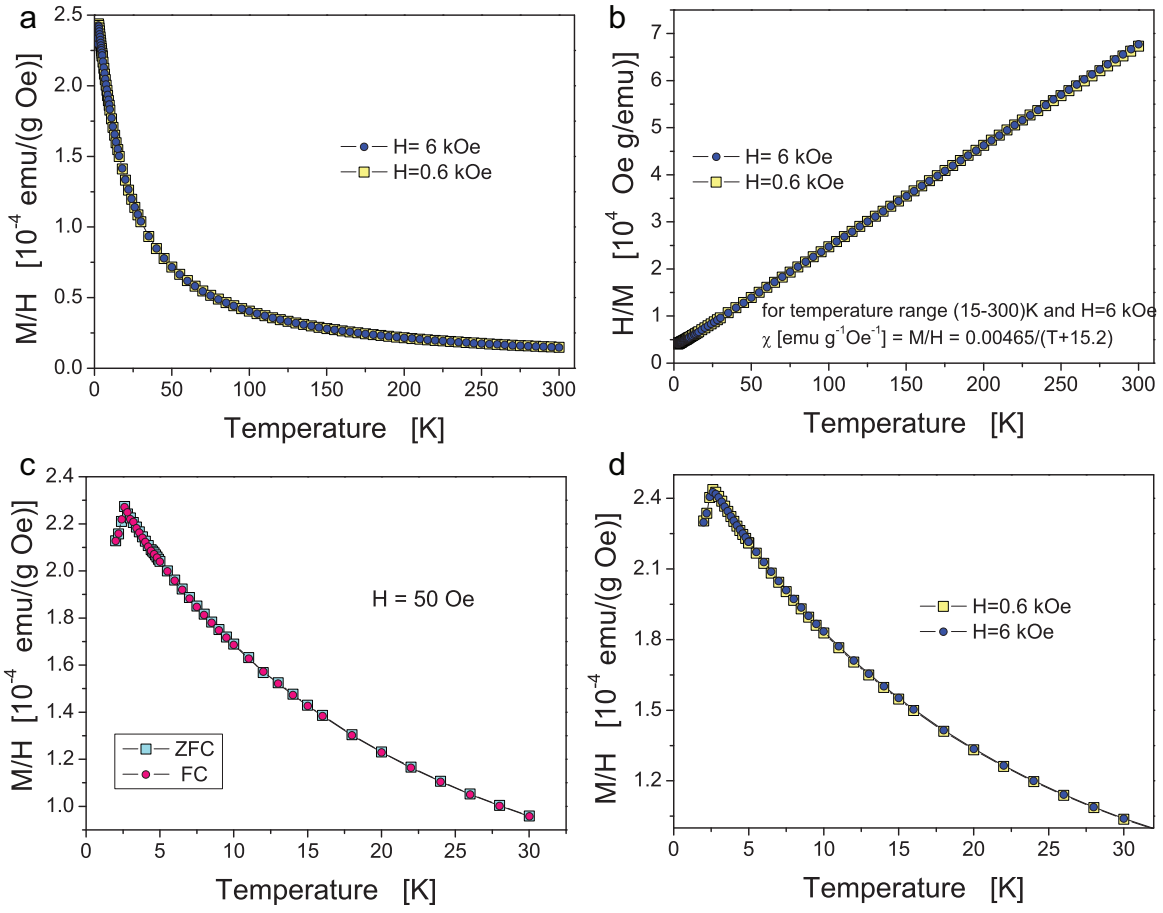

Fig. 1. Temperature dependence of the dc magnetic susceptibility (a), inverse magnetic susceptibility (b), low temperature range for $H = 50$ Oe (c) and $H = 0.6$ kOe, $H = 6$ kOe (d).

method of calcination [19]. Appropriate portions of reacting substances were homogenized by grinding and heated in air during several stages until a monophase sample was obtained or until the composition of the samples did not change after two consecutive heating stages. $Pb_2FeV_3O_{11}$ crystallizes in monoclinic symmetry with the following lattice parameters: $a = 0.56414(7)$ nm, $b = 0.74970(9)$ nm, $c = 0.7497(9)$ nm, $\beta = 81.72(1)^\circ$, $V = 0.4765$ nm^3 and $\rho_{calc} = 5.579$ g/cm^3 [19]. The values of lattice parameters for $Pb_2FeV_3O_{11}$ are essentially smaller than for other $M_2FeV_3O_{11}$ compounds with triclinic symmetry (M = Zn, Mg) while its density is higher and the melting temperature (650 °C) is essentially smaller [11,12].

The dc susceptibility measurements were carried out in the 2–300 K temperature range using an MPMS-5 SQUID magnetometer and in magnetic fields up to 50 kOe in the zero-field-cooled (ZFC) and field-cooled (FC) modes. The real χ' as well as imaginary χ'' parts of ac magnetic susceptibility were measured using mutual inductance method in an ac magnetic field of 0–10 kHz frequency range and with amplitude not exceeding 1 Oe.

The EPR spectra were recorded using a standard X-band Bruker E 500 spectrometer ($\nu = 9.45$ GHz) with magnetic field modulation of 100 kHz. The magnetic field was scaled with a NMR magnetometer. The measurements were performed in the temperature range from 3 to 290 K using an Oxford helium flow cryostat.

3. Experimental results and discussions

3.1. Dc and ac magnetic measurements

Fig. 1 shows the temperature dependence of dc magnetic susceptibility (χ) and its inverse (χ^{-1}) for the whole temperatures range as well as the magnetic susceptibility at low temperatures, obtained from dc magnetization measurements of $M_{ZFC}(T)$ for different values of an applied magnetic field. The temperature dependence of magnetic susceptibility is displaying the Curie–Weiss behavior, $\chi(T) = C/(T - T_{CW})$. The following value of the Curie–Weiss temperature is obtained: $T_{CW} = -15.2(1)$ K indicating domination of AFM interaction as shown by the negative sign of this constant. This value is significantly smaller in comparison with similar systems displaying lower symmetry $M_2FeV_3O_{11}$ (M(II) = Mg and Zn), for which $T_{CW} = -50(1)$ K (for $Mg_2FeV_3O_{11}$) and $T_{CW} = -58(1)$ K (for $Zn_2FeV_3O_{11}$) was observed [7,8]. The Curie–Weiss fit to $\chi^{-1}(T)$ data for $Pb_2FeV_3O_{11}$ yields an effective magnetic moment of $5.46(1)\mu_B$ per formulae unit. It is similar to what was obtained for samples with Zn(II) and Mg(II) ions at cation position.

At $T = 2.5$ K the dc susceptibility in FC and ZFC modes exhibits the same maximum for different applied magnetic fields (Fig. 1c and d) and no branching of FC and ZFC curves in AFM phase. This is rather different to what was registered for similar $Zn_2FeV_3O_{11}$ and $Mg_2FeV_3O_{11}$ compounds. For those compounds the splitting of the FC and ZFC magnetization curves was observed, signalling the onset of irreversibility. At higher magnetic fields ($H > 100$ Oe), the maximum in magnetization became gradually smeared out, while the irreversibility onset shifted to lower temperatures, both indicative of a spin freezing transition. Such behavior suggested significant spin frustration in the magnetic system as well as appreciable AFM correlations in the paramagnetic phase. In the presently studied $Pb_2FeV_3O_{11}$ compound the frustration phenomena seems to play a significantly smaller role. This is presumably due to the higher crystallographic symmetry of this material.

Fig. 2 shows the field dependence of the isothermal dc magnetization $M(H)$ at 2 K and 5 K. The low magnetization at low temperatures, persistent up to 50 kOe, asserts a strong AFM coupling and the concurrent compensation of some fraction of isolated trivalent iron ions in the high spin $^6S_{5/2}$ ground state. Below 2.5 K the magnetic spin correlated system is in the long-range ordered AFM state. Small curvature of the $M(H)$ curves at low temperatures complies qualitatively with the presence of a small fraction of relatively uncompensated spins or AFM clusters with reduced energy gap at low temperatures.

Fig. 3 shows the temperature dependence of the real and imaginary part of the ac susceptibility. This quantity was measured on warming up the sample after cooling down in zero magnetic field. The χ' curve shows pronounced maximum at $T_f = 2.5$ K derived at 0 Hz, 1 Hz as well as 10 kHz so it does not depend on frequency. The observed peak at 2.5 K is characteristic of the transition of the correlated spin system to the AFM state.

3.2. EPR measurements

Fig. 4 presents the EPR spectra at X-band for the $Pb_2FeV_3O_{11}$ compound registered at different temperatures in the 4–300 K range. As could be easily noticed the EPR line varies strongly with temperature what is reflected in considerable thermal dependence of the EPR line parameters: amplitude, resonance field, linewidth

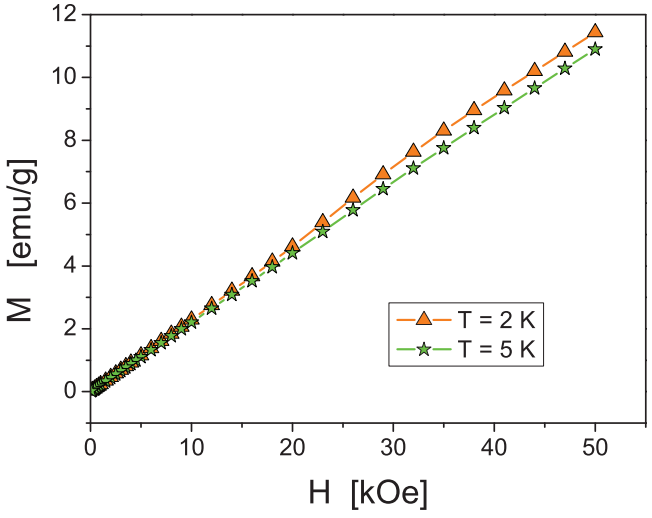

Fig. 2. Magnetic field dependence of the dc magnetic susceptibility.

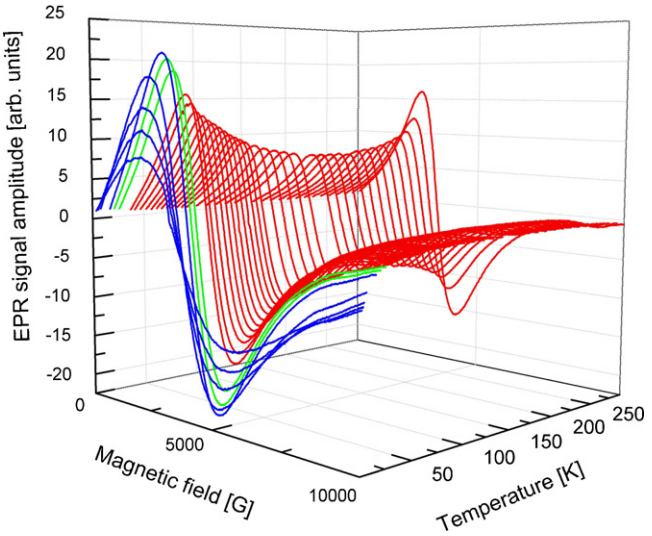

Fig. 4. Magnetic resonance spectra of iron ions in $Pb_2FeV_3O_{11}$ compound registered at different temperatures.

and integrated intensity. The high temperatures region is dominated by nearly symmetrical, very intense and broad resonance line centered at $g_{eff} \sim 2.0$ that could be attributed to the Fe^{3+} ions. Below 5 K a very small concentration of isolated iron ions in the high spin state is also detected. The shape of the EPR resonance lines could be very well fitted by the Lorentzian function. Because the line is very broad the contribution from the negative magnetic fields has to be taken into account. This is the consequence of the linearly polarized resonance field that is important when the linewidth becomes comparable to the resonance field.

Fig. 5 presents the temperature dependence of the resonance field B_r (right axis) and associated with it an effective g-factor, $h\nu = g_{eff}\mu_B B_r$, for the broad and intense line. The temperature dependence of B_r has different character than for previously investigated $M_2FeV_3O_{11}$ (M(II) = Mg and Zn) compounds [7,8]. The temperature gradient of that field ($\Delta H_r/\Delta T$) has the following values in the three different temperature ranges: $\Delta B_r/\Delta T$ (290–45 K) = 0.3(1) G/K, $\Delta B_r/\Delta T$ (45–20 K) = 2.1(1) G/K, and $\Delta B_r/\Delta T$ (20–4 K) = 15.0(3) G/K. An essential decrease of that value was observed at the Currie–Weiss temperature for $M_2FeV_3O_{11}$ (M(II) = Mg and Zn) compounds. This change is related to the reorientation processes in the correlated spins that changes the spins resonance condition, $h\nu = g\mu_B(B_o \pm B_{int})$, where h is Planck constant, ν is resonance frequency, μ_B is Bohr magneton, B_o is an external magnetic field and B_{int} is an internal magnetic field created by the spin system. For the β-$Cu_3Fe_4V_6O_{24}$ compound the following values were obtained: $\Delta B_r/\Delta T$(290–85 K) = 0.08(5) G/K, $\Delta B_r/\Delta T$(60–28 K) = 2.3(2) G/K and $\Delta B_r/\Delta T$(28–11 K) = −22.9(1) G/K [20]. These values are essentially different than those obtained for the $Pb_2FeV_3O_{11}$ compound and the most important result is that this gradient changes the sign at low temperatures. The value of the resonance field gradient is much greater in the high temperatures range, comparable in the 60–28 K range where it is almost two times smaller. For the $M_3Fe_4V_6O_{24}$ (Mg and Mn) compounds an opposite trend is registered [9,10]. The system $M_3Fe_4V_6O_{24}$ has a less crystallographically disordered structure than the $M_2FeV_3O_{11}$ system [11–14].

Introduction of copper(II) ions at the cation positions could induce ferromagnetic interaction which at low temperatures could alter the sign of the resonance field gradient.

Fig. 6 presents the temperature dependence of the linewidth in the whole temperature range. The linewidth increases with the decrease in temperature from the RT. This increase is especially pronounced at low temperatures, below 30 K. The inset in Fig. 6 shows the temperature dependence of the peak-to-peak linewidth in double logarithmic scale. Although in general not linear, two linear segments could be recognized – one at low temperatures ($T < 10$ K) and the other at high temperatures ($T > 150$ K). Thus in the low temperature range $\Delta B_{pp} \sim T^{-0.52}$, while in the high temperature range $\Delta B_{pp} \sim T^{-0.21}$. Comparison of the temperature dependence of linewidth and resonance field reveals a considerable similarity of both dependences. To display this interrelation a double logarithmic plot of linewidth and resonance field is presented in Fig. 7. In a wide temperature range (4–160 K) the experimental points align along a single straight line.

The temperature dependence of EPR line amplitude A_{pp} is rather peculiar. It is presented in Fig. 8. The amplitude decreases initially with decrease in temperature from RT and reaches a wide minimum at 175 K. On further cooling the amplitude increases to reach a sharp maximum at 12.3 K. Below this temperature the amplitude strongly decreases down to the lowest available temperature in EPR measurements (4 K). That peculiar shape of A_{pp}(T) curve indicates on the existence of different AFM pairs of Fe^{3+} ions. In particular the low temperature maximum might be a fingerprint of weakly coupled iron pairs and the presumed maximum above room temperatures (unobserved) of a strongly coupled iron pairs with a singlet ground state. The solid line in Fig. 8 is the best fit to the experimental points of an expression suitable for such situation and describes the data very well. The obtained value of the exchange constant for weak and strongly coupled pairs is $J_1 = 17$ K and $J_2 = 427$ K, respectively. The existence of two different subsystems of iron dimers in the $Pb_2FeV_3O_{11}$ compound might be related to the expected two different crystallographic positions of

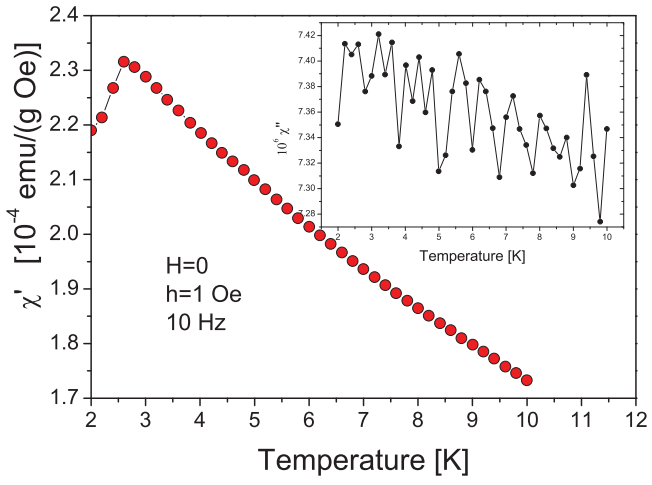

Fig. 3. Temperature dependence of complex ac magnetic susceptibility: real part and imaginary part (inset).

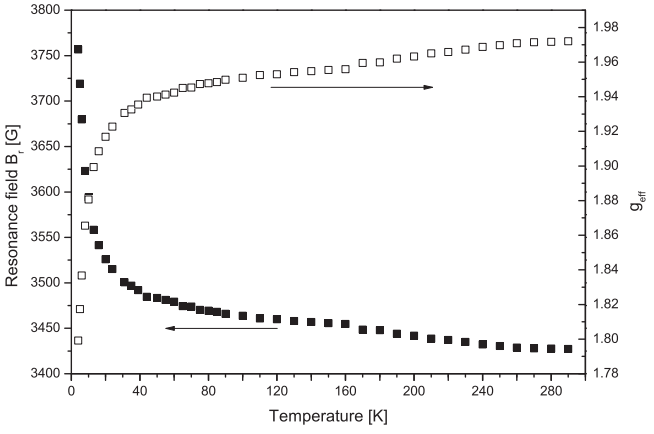

Fig. 5. Temperature dependence of the resonance field B_r (right axis) and an effective g-factor g_{eff} (left axis).

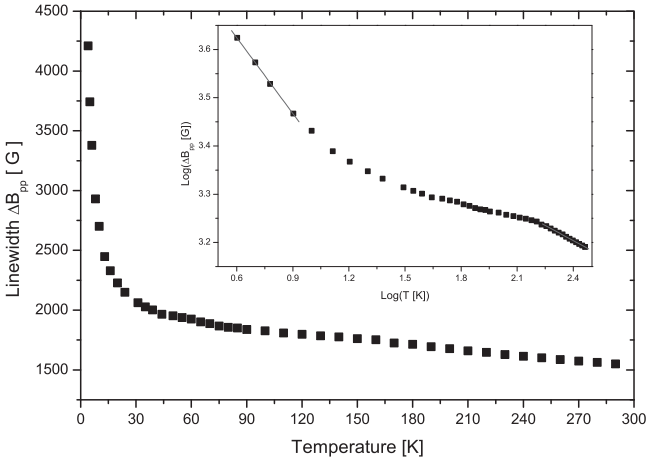

Fig. 6. Temperature dependence of the linewidth ΔB_{pp} and the same dependence in double logarithmic scale (inset). The solid straight lines in the inset are the least-squares fits in low and high temperature ranges.

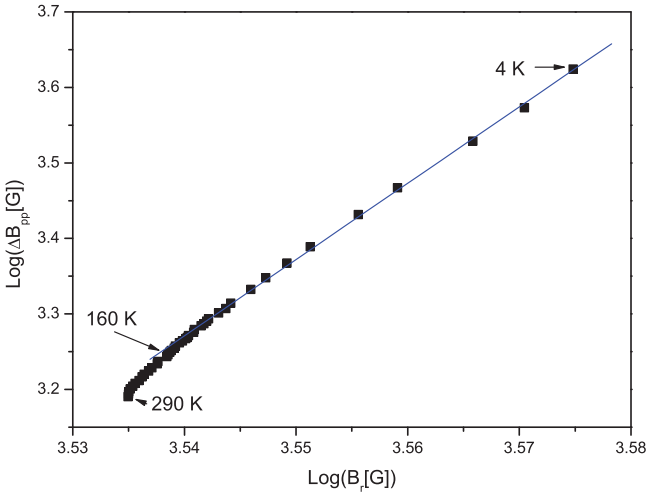

Fig. 7. A double logarithmic plot of linewidth ΔB_{pp} vs resonance field B_r.

Fe ions in the $Pb_2FeV_3O_{11}$ structure. A similar situation was already observed in another vanadate β-$Cu_3Fe_4V_6O_{24}$ [20].

In Fig. 9a (left axis) the temperature dependence of yet another important parameter – EPR integrated intensity, I_{EPR}, is presented. The EPR integrated intensity

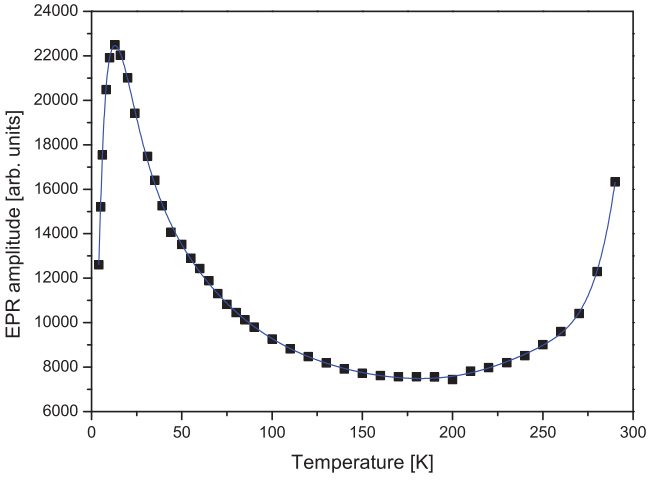

Fig. 8. Temperature dependence of the EPR signal amplitude A_{pp}. The solid line is the least-squares fit assuming the existence of two kinds of the AFM iron pairs.

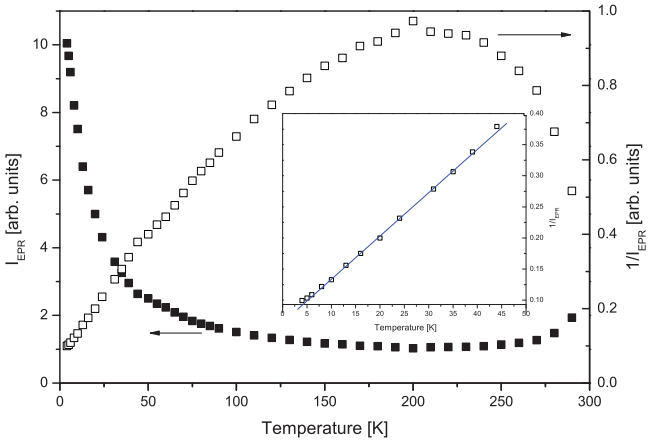

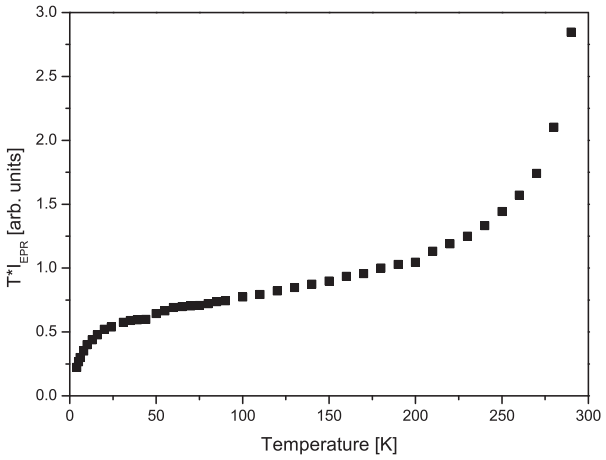

Fig. 9. Temperature dependence of the EPR integrated intensity I_{EPR} (right axis), inverse of the EPR integrated intensity I_{EPR}^{-1} (left axis) (a) and the product $I_{EPR}{}^{*}T$ (b). The inset in (a) shows $I_{EPR}^{-1}(T)$ dependence in the low temperature range with the least-square fit by straight line (solid line).

is usually calculated as the area under the absorption curve or the product of signal amplitude and square of the linewidth, $I_{EPR'} = A_{pp}(\Delta B_{pp})^2$. In case of large temperature changes of the g-factor of the resonance line and a field-sweep experiments (as in our case) this definition should be supplemented by that g-factor so for calculation of the EPR integrated intensity we used the following equation: $I_{EPR} = g_{eff}A_{pp}(\Delta B_{pp})^2$ [21]. EPR integrated intensity is proportional to the dynamic magnetic susceptibility of the spin system at microwave frequency. On cooling $Pb_2FeV_3O_{11}$ from RT the integrated intensity decreases slightly to reach a shallow minimum at about 200 K and on further cooling starts to increase. This increase of I_{EPR} with temperature decrease is considerable in the low temperature range below 50 K. Surprisingly, no maximum of I_{EPR} is observed in that temperature range. In the same Fig. 9a (right axis) the temperature dependence of the inverse of EPR integrated intensity, I_{EPR}^{-1} is presented. The low temperature part of I_{EPR}^{-1} (between 10 and 45 K) could be approximated by a straight line (see inset in Fig. 9a). It means that the Curie–Weiss law, $I(T) = C/(T - T_0)$, is in operation with $T_0 = -9.5$ K in that temperature range. The negative sign of T_0 indicates on AFM interactions in the observed spin system. Below 10 K the I_{EPR}^{-1} points deviate slightly from the Curie–Weiss line (see inset in Fig. 9a).

In Fig. 9b the temperature dependence of the product TI_{EPR} is presented. This product is proportional to the square root of an effective magnetic moment. Decrease of TI_{EPR} on cooling is the evidence of domination of the AFM interactions in the whole investigated temperature range. This decrease is especially noticeable in the high temperature range, where the strong pairs depopulate higher energy levels and in the low temperature range where the weak pairs fall down on the singlet ground level and do not participate in the magnetic resonance.

As a result of the EPR studies the following picture of the spin system in $Pb_2FeV_3O_{11}$ emerges: there are three different magnetic entities involving iron ions: isolated Fe^{3+} ions, weak AFM iron pairs ($J_1 = 17$ K), and strong AFM iron pairs ($J_2 = 427$ K). Without a well-defined crystallographic structure being available any detailed interpretation of magnetic behavior at the molecular level is not possible. One can only speculate that two different crystallographic positions of Fe ions exist in $Pb_2FeV_3O_{11}$ structure.

Comparison of the results of magnetic susceptibility and magnetic resonance measurements shows important differences. Similar differences were detected in studies of other compounds [22]. They all stem from the fact that EPR measures

dynamic properties of the spin system at frequency of approximately 10^{10} Hz in contrast to dc magnetic susceptibility that is a static method. The spin system of $Pb_2FeV_3O_{11}$ orders antiferromagnetically at $T_N = 2.5$ K and this long rang order is reflected in dc susceptibility measurements. The precursors of that state in form of spin pairs or clusters are observed at higher temperatures by the EPR technique. Thus both methods could be regarded as complementary, delivering information on different aspects of the observed spin system.

4. Conclusions

A significantly more magnetic homogeneity has been found in $Pb_2FeV_3O_{11}$ than in other $M_2FeV_3O_{11}$ (M(II) = Mg and Zn) compounds. In the high temperature range AFM interaction with the Curie–Weiss temperature $\theta = -15.3$ K has been measured which is smaller than obtained for other M–Fe–V–O systems. Magnetization measurements at different applied magnetic fields revealed the presence of paramagnetic-AFM phase transition at $T_N = 2.5$ K. EPR measurements uncovered a complicated picture of single iron ions and iron pairs or clusters existing in the paramagnetic phase. Temperature dependence of the EPR signal suggests that besides isolated Fe^{3+} ions, two kinds of AFM pairs exist: weakly coupled Fe^{3+}–Fe^{3+} pairs with the exchange constant $J_1 = 17$ K, and strongly coupled iron pairs with $J_2 = 427$ K. The EPR method seems to be complementary to the magnetic susceptibility measurements in obtaining a more detailed picture of magnetic interaction in the $Pb_2FeV_3O_{11}$ compound.

References

[1] W.D. Harding, H.H. Kung, V.L. Kozhernik, K.R. Poeppelmeier, J. Catal. 144 (1993) 597.
[2] M.A. Lafontaine, J.M. Greneche, Y. Laligant, G. Ferey, J. Solid State Chem. 108 (1994) 1.
[3] S.A. Korili, S. Ruiz, B. Delmon, Catal. Today 32 (1996) 229.
[4] X. Wang, D.A. Vander Griend, C.L. Stern, K.P. Poeppelmeir, J. Alloys Compd. 298 (2000) 119.
[5] P. Rybarczyk, H. Berndt, J. Radnik, M.–M. Pohl, O. Buyerskaya, M. Baerns, A. Bruckner, J. Catal. 202 (2001) 45.
[6] L.E. Briand, J.-M. Jehng, L. Cornaglia, A.M. Hirt, I.E. Wachs, Catal. Today 78 (2003) 257.
[7] V. Likodimos, N. Guskos, S. Glenis, R. Szymczak, A. Bezkrovnyj, M. Wabia, J. Typek, M. Kurzawa, I. Rychlowska-Himmel, A. Blonska-Tabero, Eur. Phys. J. B 38 (2004) 13.
[8] N. Guskos, V. Likodimos, J. Typek, G. Zolnierkiewicz, R. Szymczak, A. Blonska-Tabero, J. Non-Cryst. Solids 352 (2006) 4179.
[9] N. Guskos, V. Likodimos, S. Glenis, G. Zolnierkiewicz, J. Typek, R. Szymczak, A. Blonska-Tabero, J. Appl. Phys. 101 (2007) 103922.
[10] N. Guskos, H. Ohta, G. Zolnierkiewicz, S. Okubo, Wei-min Zhang, J. Typek, C. Rudowicz, R. Szymczak, M. Bosacka, T. Nakamura, J. Non-Cryst. Solids 355 (2009) 1419.
[11] N. Guskos, M. Wabia, M. Kurzawa, A. Bezkrovnyj, J. Typek, I. Rychlowska-Himmel, A. Blonska-Tabero, Radiat. Eff. Defects Solids 158 (2003) 369.
[12] N. Guskos, J. Typek, BezkrovnyjF A., V. Likodimos, M. Wabia, M. Kurzawa, E.A. Anagnostakis, G. Gasiorek, J. Alloys Compd. 377 (2004) 47.
[13] N. Guskos, A. Bezkrovnjj, J. Typek, N.Yu. Ryabova, A. Blonska-Tabero, M. Kurzawa, M. Maryniak, J. Alloys Compd. 391 (2005) 20.
[14] A. Beskrovnyy, N. Guskos, J. Typek, N.Yu. Ryabova, A. Blonska-Tabero, M. Kurzawa, G. Zolnierkiewicz, Rev. Adv. Mater. Sci. 12 (2006) 166.
[15] G. Zolnierkiewicz, N. Guskos, J. Typek, A. Blonska-Tabero, Acta Phys. Pol. A 109 (2006) 675.
[16] G. Zolnierkiewicz, N. Guskos, J. Typek, E.A. Anagnostakis, A. Blonska-Tabero, M. Bosacka, J. Alloys Compd. 471 (2009) 28.
[17] N. Guskos, J. Typek, G. Zolnierkiewicz, A. Blonska-Tabero, M. Kurzawa, S. Los, W. Kempinski, Mater. Sci.-Pol. 24 (2006) 985.
[18] N. Guskos, V. Likodimos, S. Glenis, J. Typek, J. Majszczyk, G. Zolnierkiewicz, A. Blonska-Tabero, C.L. Lin, Rev. Adv. Mater. Sci. 14 (2007) 85.
[19] A. Blonska-Tabero, Mater. Res. Bull. 44 (2009) 1621.
[20] N. Guskos, G. Zolnierkiewicz, J. Typek, R. Szymczak, P. Berczynski, A. Blonska-Tabero, J. Non-Cryst. Solids, in press.
[21] T. Gruner, J. Wykhoff, J. Sichelschmidt, C. Krellner, C. Geibel, F. Steglich, J. Phys.: Condens. Matter 22 (2010) 135602.
[22] M. Ruitenbeek, A. Barbon, E.E. van Faassen, J.W. Geus, Catal. Lett. 54 (1998) 101.